Meron configurations in easy-plane chiral magnets

David Bachmann,[1] Michail Lianeris,[2,3,4] and Stavros Komineas[2,3,*]

[1]*Physikalisches Institut, Albert-Ludwigs-Universität Freiburg, Hermann-Herder-Str. 3, D-79104 Freiburg, Germany*
[2]*Department of Mathematics and Applied Mathematics, University of Crete, 70013 Heraklion, Crete, Greece*
[3]*Foundation for Research and Technology (FORTH), 70013 Heraklion, Crete, Greece*
[4]*Department of Electrical and Information Engineering, Polytechnic University of Bari, 70126 Bari BA, Italy*

(Received 3 May 2023; revised 19 June 2023; accepted 22 June 2023; published 5 July 2023)

We demonstrate the existence and study in detail the features of chiral bimerons which are static solutions in an easy-plane magnet with the Dzyaloshinskii-Moriya interaction. These are skyrmionic textures with an integer topological charge, and they present essential analogies to the meron configurations introduced in the context of quark confinement in the O(3) nonlinear σ model. We employ a Möbius transformation to show that, for weak chirality, bimeron configurations approach Belavin-Polyakov solutions characterized by tightly bound vortex and antivortex parts of the same size. Stronger chirality induces a larger difference in the vortex and antivortex sizes and also a detachment of merons, suggesting the possibility for a topological phase transition. Exploiting the fact that bimerons of opposite topological charges may exist in the same material, we demonstrate numerically a mechanism to generate meron pairs.

DOI: 10.1103/PhysRevB.108.014402

I. INTRODUCTION

Merons are localized configurations that possess one-half topological charge, and they are relevant in theories ranging from high-energy physics to condensed matter. Their name reflects the fact that a meron can be considered as a part (greek: $\mu\epsilon\rho o\varsigma$) of a soliton with an integer topological charge [1,2]. For large distances or large couplings, the formation of merons is favored due to their logarithmically divergent energy, and they are considered to offer a possible mechanism leading to quark confinement.

In magnetic films with the chiral Dzyaloshinskii-Moriya (DM) interaction, topological solitons with integer-valued topological charge are magnetic *skyrmions* [3–5]. Merons were introduced in the context of the nonlinear O(3) σ model, a prototype model corresponding to the time-independent Landau-Lifshitz equation, in Ref. [2]. Under *Möbius transformations*, an axially symmetric skyrmion of topological charge equal to unity is decomposed into two spatially separated merons that may have different sizes.

We study chiral ferromagnets with *easy-plane anisotropy* which support skyrmionic configurations consisting of two merons, known as *bimerons* [6–13]. Bimeron structures have also been studied in antiferromagnets [14,15] and in nonchiral magnets [16–19]. The two constituent parts are a vortex and an antivortex of different polarities, each contributing one-half of the topological charge. While a single vortex may be energetically favored by the DM interaction, it is a challenging problem whether a composite configuration including vortices of both windings, i.e., a vortex and an antivortex, yields a stable configuration.

Bimeron structures have been observed in confined geometries [8,19] as well as in antiferromagnetic $\alpha-Fe_2O_3$ films [20]. Observations of square lattices of chiral merons [21] have been reported in Ref. [22], and their stabilization was investigated within a Ginzburg-Landau model [23].

The chiral bimerons presented here are directly related to the meron configurations constructed in Ref. [2]. First, the configuration is asymmetric (the two merons have different sizes), and a Möbius transformation gives a skyrmion including two scales. Second, tuning the chirality parameter allows detaching of the constituent parts. A further remarkable feature is that the far field of the chiral bimeron is algebraic, like the O(3) σ model, despite the presence of anisotropy which typically induces exponential decay.

We exploit the possible coexistence of oppositely charged bimerons in DM magnets, and we numerically demonstrate a remarkable process for the smooth generation of a bimeron. A straightforward iteration of this mechanism can yield a proliferation scheme for bimerons that overcomes topological constraints, opening the possibility for a topological phase transition such as the Berezinskii-Kosterlitz-Thouless (BKT) transition.

The paper is organized as follows. In Sec. II, the model for easy-plane chiral ferromagnets is presented. In Sec. III, the numerical solutions for bimerons are given. In Sec. IV, details of the bimeron profile are discussed, and the relation to the O(3) merons is quantified. In Sec. V, a mechanism for the generation of bimerons is discussed. Section VI contains our concluding remarks.

*komineas@uoc.gr

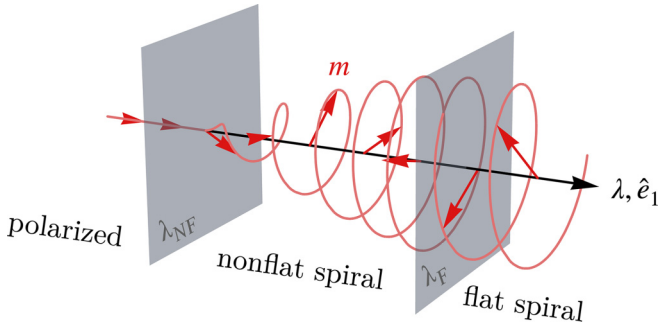

FIG. 1. Ground states and phase transitions for an easy-plane chiral ferromagnet vs model parameter λ. We have the polarized state for $\lambda < \lambda_{\rm NF}$, a nonflat spiral for $\lambda_{\rm NF} < \lambda < \lambda_{\rm F}$, and a flat spiral for $\lambda > \lambda_{\rm F}$.

II. EASY-PLANE CHIRAL MAGNETS

We consider a ferromagnetic film with easy-plane anisotropy and the DM interaction. The magnetic energy is

$$E = A\int \partial_\mu \mathbf{m}\cdot\partial_\mu \mathbf{m}\, d^2x + K\int m_3^2\, d^2x + D\int \hat{\mathbf{e}}_\mu\cdot(\partial_\mu \mathbf{m}\times\mathbf{m})\, d^2x, \tag{1}$$

where $\mathbf{m} = (m_1, m_2, m_3)$ is the normalized magnetization vector, $\mu = 1, 2$, $\hat{\mathbf{e}}_\mu$ denotes the unit vectors in the respective directions, A is the symmetric exchange parameter, K is the anisotropy parameter, and D is the DM or antisymmetric exchange parameter.

The dynamics of the magnetization vector is described by the Landau-Lifshitz equation as obtained from the energy functional Eq. (1). Using $\ell_{\rm w} = \sqrt{A/K}$ as the unit of length, we obtain the dimensionless form:

$$\partial_\tau \mathbf{m} = -\mathbf{m}\times\mathbf{h}_{\rm eff} + \alpha\mathbf{m}\times\partial_\tau\mathbf{m}, \tag{2}$$

where we include Gilbert damping with parameter α, and the effective field reads

$$\mathbf{h}_{\rm eff} = \Delta\mathbf{m} - m_3\hat{\mathbf{e}}_3 - 2\lambda(\hat{\mathbf{e}}_\mu\times\partial_\mu\mathbf{m}) \tag{3}$$

and includes the dimensionless DM parameter:

$$\lambda = \frac{D}{2\sqrt{AK}}. \tag{4}$$

This model appears to be like that for easy-axis ferromagnets where a spiral is the ground state for a strong enough DM interaction [3]. In this spiral solution, the magnetization vector rotates in the plane perpendicular to the direction in which the magnetization varies; hence, we may call this a *flat* spiral. Despite the apparent similarity of the models, the present case of easy-plane anisotropy allows for an additional phase [24], where the phase transitions occur at two critical values of the DM parameter [25]:

$$\lambda_{\rm NF} = \tfrac{1}{2}, \quad \lambda_{\rm F} \approx 0.705. \tag{5}$$

As illustrated in Fig. 1, for a weak DM interaction, $\lambda < \lambda_{\rm NF}$, the fully *polarized* state is the ground state with the magnetization vector aligning with an easy-plane direction (without loss of generality, we may assume $\mathbf{m} = \hat{\mathbf{e}}_1$). By increasing λ, we enter an intermediate phase in the form of a *nonflat* spiral at $\lambda = \lambda_{\rm NF}$. The spiral presents a rotation of the projection of $\mathbf{m}$ on the $\hat{\mathbf{e}}_2$-$\hat{\mathbf{e}}_3$ plane as we move along the x axis, and at the same time, the component m_1 oscillates around a nonzero value. The period of the spiral tends to infinity for $\lambda \to \lambda_{\rm NF}$ (from above), while the component m_1 approaches unity in the same limit. As λ increases above $\lambda_{\rm NF}$, m_1 decreases, and it vanishes at $\lambda = \lambda_{\rm F}$, where the flat spiral is obtained with $\mathbf{m}$ perpendicular to $\hat{\mathbf{e}}_1$ and rotating in the $\hat{\mathbf{e}}_2$-$\hat{\mathbf{e}}_3$ plane. For $\lambda > \lambda_{\rm F}$, the flat spiral is the ground state, and its period decreases with increasing λ.

III. BIMERON SOLUTIONS

In a magnetic film (a two-dimensional system), skyrmionic textures [26–29] and vortices are excited states above the polarized state in the regime $0 < \lambda < \lambda_{\rm NF}$. For vortices, the winding of the in-plane magnetization vector, as we rotate around the vortex center, may follow the same or the opposite sense of rotation. We define accordingly the *winding number* or *vortex number* $\kappa = \pm 1$. We call *vortices* those with a positive winding number and *antivortices* those with a negative winding number. The sign of the out-of-plane component of the magnetization in the central region of the vortex (vortex core) defines the vortex *polarity*. For a vortex with positive winding, the orientation of the in-plane magnetization component with respect to the radial direction gives the *helicity*.

In chiral magnets, certain vortex configurations are energetically favored by the DM interaction, as this gives a negative contribution for particular swirling magnetic configurations. This is analogous to the effect of the DM interaction for skyrmions. This means that a vortex (or a skyrmion) with only one of the two possible windings can be an energy minimum. Specifically, for the energy as given in Eq. (1), vortices are favored for positive polarity and helicity $-\pi/2$ or negative polarity and helicity $\pi/2$. Regarding the vortex profile, it is an unusual fact that the magnetization field for a chiral vortex decays following a power law, as shown by standard asymptotic analysis [25]. This is due to the DM interaction and despite the presence of anisotropy that typically gives exponential decay for vortex configurations. No isolated static antivortex solutions are found within the model described by Eq. (1).

Magnetic configurations are characterized by the *skyrmion number* defined as

$$Q = \frac{1}{4\pi}\int q\, d^2x, \quad q = \mathbf{m}\cdot(\partial_1\mathbf{m}\times\partial_2\mathbf{m}), \tag{6}$$

where q is a *topological density*, and it plays the role of the local vorticity. Vortices have $Q = \pm\frac{1}{2}$, where the sign depends on their winding number and polarity. The question arises whether solutions that represent stable skyrmions, i.e., topological solitons with an integer skyrmion number, are possible in the easy-plane case.

Skyrmionic textures with $Q = \pm 1$ may be constructed from a vortex paired with an antivortex of opposite polarity. Using the *stereographic projection* of the magnetization vector:

$$\Omega = \frac{m_1 + im_2}{1 + m_3}, \tag{7}$$

such configurations are given by the rational map:

$$\Omega_\mu = \frac{z - ia_1}{z - ia_2}, \tag{8}$$

where $a_1, a_2 \in \mathbb{R}$, and $z = x + iy$ is the position variable on the complex plane, gives a vortex centered at position $(x, y) = (0, a_1)$ and an antivortex centered at $(0, a_2)$. Since the absolute position of the resulting two-vortex configuration can be shifted by simple spatial translations, only their separation, given by the difference $a_1 - a_2$, is significant. The vortex exhibits a positive out-of-plane magnetization, i.e., $m_3 > 0$, whereas the antivortex is characterized by $m_3 < 0$.

Within the O(3) nonlinear σ model, configurations obtained by rational maps such as in Eq. (8) are exact solutions. Solutions described by Eq. (8) necessarily feature symmetric vortex and antivortex configurations having the same size. The two vortices are considered merons, each occupying one-half of the plane. Consequently, we can assign to each meron a radius (assume $a_1 > a_2$):

$$R = \frac{a_1 - a_2}{2}. \tag{9}$$

To find static bimerons, we apply an energy minimization algorithm. This is equivalent to simulating Eq. (2) with maximum damping. Due to the long range of bimeron configurations, we employ *stretched coordinates* ξ, η, where $x = \tan\xi$, $y = \tan\eta$ with $-\pi/2 < \xi, \eta < \pi/2$, resulting in a lattice in x, y with nonuniform spacing that effectively extends to infinity in all directions. We typically use a 400×400 square lattice with a minimum spacing of 0.08 (in dimensionless units) at the origin.

We use as an initial condition the form of Eq. (8). The numerical relaxation results in *asymmetric* meron pairs, i.e., two merons of different sizes. Figure 2 shows two example configurations obtained for two different values of the parameter λ. The vortex has an almost axially symmetric profile around its center, while the antivortex is elongated. The elongation is more pronounced for larger values of λ, as in Fig. 2(a), while the antivortex profile is getting closer to an axially symmetric one for lower values of λ, as in Fig. 2(b).

The antivortex elongation has been noted in Refs. [6,7], and it is apparent in numerical results showing vortex collections in Ref. [28]. In Ref. [30], an elongated vortex is found as an exact solution in a specific solvable σ model with DM interaction and easy-plane anisotropy. The apparent similarity is promising to explain the present numerical results, but the connection of the model in Eq. (2) with the solvable σ model is not straightforward.

We find that the bimeron solutions exhibit an algebraically (power law) decaying far field with $|\Omega| \sim 1/r^2$. The algebraic decay is shared with the merons of Eq. (8) for the O(3) model, which actually give $|\Omega| \sim 1/r$. A corresponding result is found by standard asymptotic analysis that gives an algebraic behavior for a single chiral vortex configuration [25]. The power law for a single vortex or a bimeron configuration is an unusual behavior as the presence of anisotropy typically induces exponential decay in vortex configurations.

While $m_3 < 0$ at the antivortex core region, m_3 becomes positive in a region well below the antivortex. The domain with $m_3 > 0$ can be discerned in Fig. 2 by the change in the color well below the antivortex core region. For example, for $\lambda = 0.4$, we have $m_3 > 0$ below $y = -3.43$ on the y axis. This feature represents a difference between the chiral bimeron configuration and the configuration in Eq. (8) at large distances.

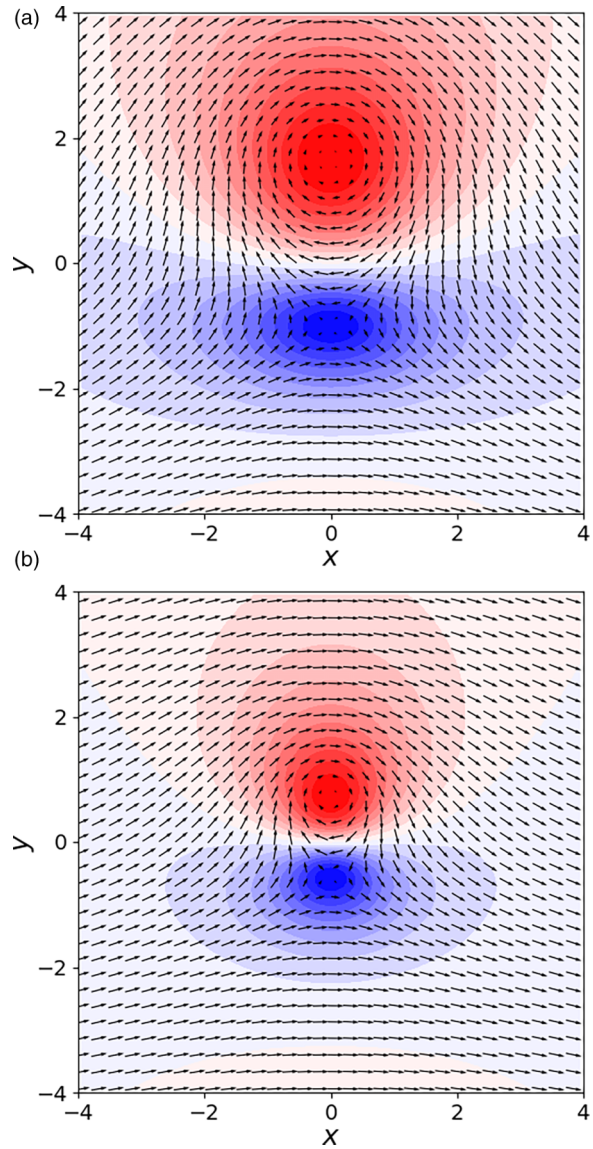

FIG. 2. Static bimeron solution of the model given in Eq. (2). Vectors show the projection of the magnetization (m_1, m_2) on the plane. Contour plots for m_3 are colored, where red indicates $m_3 > 0$ and blue indicates $m_3 < 0$. The center of the bimeron, defined to be at the point where $m_1 = -1$, is at the origin. The skyrmion number is $Q = 1$. (a) A bimeron for parameter value $\lambda = 0.4$. The centers of the vortex and antivortex, defined to be at the point where $m_3 = \pm 1$, are located on the y axis, at $y = 1.66$ and -1.01, respectively, in units of ℓ_w. (b) A bimeron for $\lambda = 0.32$. The vortex center is at $y = 0.71$ and the antivortex at $y = -0.56$.

Bimeron solutions are found for a range of parameter values. We present results for bimeron configurations down to $\lambda = 0.28$. It is numerically challenging to find bimeron solutions for small λ as an increasingly finer spatial resolution would be needed. Figure 3 shows the distances of the vortex

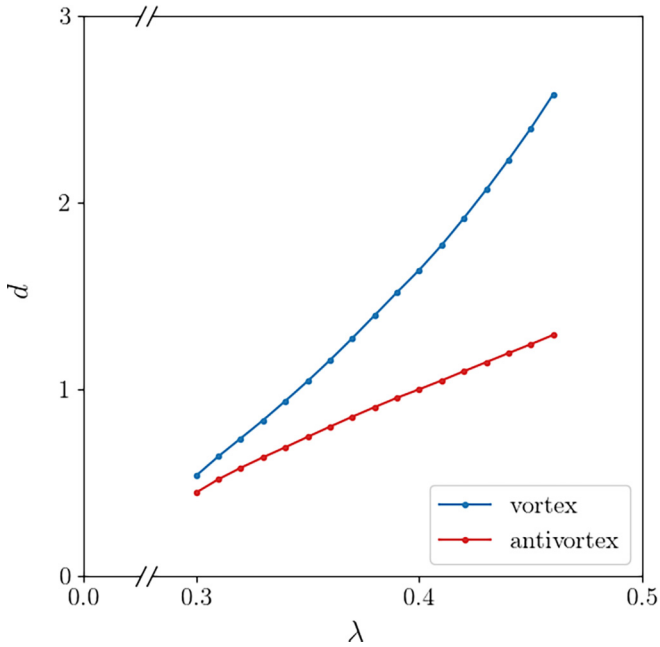

FIG. 3. Distances of the vortex (upper, blue line) and the antivortex (lower, red line) centers from the bimeron center as a function of the parameter λ. Points present numerical results, connected by solid lines. For small λ, the vortex and the antivortex are progressively placed more symmetrically on either side of the bimeron center. For $\lambda \geqslant 0.5$, at the point of transition to the nonflat spiral, the vortex is expected to get completely detached.

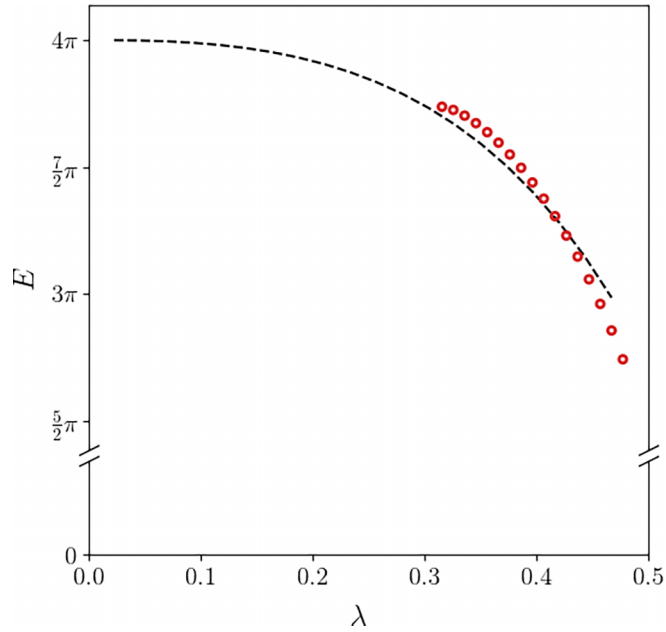

FIG. 4. The energy of the bimeron as a function of the parameter λ. Results from numerical simulations are given by circles. The dotted line shows the asymptotic result as obtained analytically in Eq. (10) for the axially symmetric skyrmions, and it is shown for comparison.

and antivortex centers (the points where $m_3 = \pm 1$) from the bimeron center (the point where $m_1 = -1$) as λ is varied. As the value of λ decreases, the centers of the vortex and antivortex approach each other, and they move progressively to locations symmetrically placed on opposite sides of the bimeron center.

We expect that bimerons exist down to $\lambda \to 0$. In this limit, the DM and anisotropy energy terms decrease, and the exchange term dominates. Thus, the configuration is expected to approach the rational map given in Eq. (8) with a decreasing distance between the merons, that is, $a_1 - a_2 \to 0$. This picture is supported by the results in Fig. 3. The issue is discussed further in Sec. IV.

A larger parameter λ gives a larger separation between the two merons. After the phase transition to the nonflat spiral, for $\lambda \geqslant \lambda_{\rm NF} = \frac{1}{2}$, we expect no bimeron solutions. Specifically, for $\lambda \geqslant \lambda_{\rm NF}$, a single vortex has negative energy [25], and it is expected to detach completely from the antivortex. As seen in Fig. 3, this behavior is supported by the numerical simulations which converge to bimeron configurations with increasing meron separation as $\lambda \to \lambda_{\rm NF}$.

Figure 4 shows the energy of the bimeron as a function of the parameter λ. The DM and anisotropy energies decrease in absolute value, and they go to zero (from negative and positive values, respectively) as $\lambda \to 0$, and the bimeron size goes to zero, too. The exchange energy decreases, and it approaches the value 4π for $\lambda \to 0$, which is the value for the bimeron profile in Eq. (12). For small λ, the total energy approaches the value $E = 4\pi$, thus supporting the argument that the bimeron configuration is given by Eq. (12) with $a \to 0$. A similar situation has been studied for the axially symmetric skyrmion where the asymptotic result for the energy is [31,32]

$$E = 4\pi\left(1 + \frac{\lambda^2}{\ln \lambda}\right), \quad \lambda \ll 1. \tag{10}$$

In Fig. 4, we tentatively plot Eq. (10), and we find that it is in agreement with the present numerical results for small λ. This can be explained by the fact that the exchange interaction is dominant for $\lambda \ll 1$, and the arguments of Refs. [31,32] for the asymptotic calculation of the energy can also be applied in the present case. For larger λ, the energy decreases. The results in Fig. 4 indicate that the energy attains a positive value at $\lambda = \lambda_{\rm NF} = 0.5$. For $\lambda > \lambda_{\rm NF}$, the bimeron is not expected to be stable, as explained earlier. A phase transition to a nonflat spiral will occur at that point, and the energy would drop discontinuously to negative values. A full mathematical treatment of these issues would be needed to obtain precise results for the phase transitions at $\lambda \to 0$ and $\lambda \to \lambda_{\rm NF}$, but this is beyond the scope of this paper.

The fact that the vortex and antivortex are centered on the y axis for all bimerons presented here, such as in Fig. 2, is dictated by the choice of the far field magnetization $\mathbf{m} = \hat{\mathbf{e}}_1$, that is, by the choice for the spontaneously broken symmetry. If the bimeron configuration would be rotated in space, keeping the far field fixed, this would necessarily have to be accompanied by a change of the helicity of the vortex and thus an increase of the DM energy. A related fact is that chiral bimerons have been found here as static solutions within the easy-plane magnet, in contrast to vortex-antivortex dipoles in standard models (without the chiral interaction) where the pair is necessarily nonstatic, i.e., rotating [33,34]. These striking features of chiral bimerons originate in the invariance of the

DM interaction under simultaneous rotations in real and magnetization space.

We have repeated the simulations including the magnetostatic field, and we have verified that the bimeron pair exists in this case, too. Therefore, bimerons can be realistically expected to be observed experimentally in a magnetic material with easy-plane anisotropy and chiral interaction.

All calculations in this paper have been performed for the bulk type of DM interaction used in Eq. (1). Equivalent bimeron solutions can be found for other types of DM interactions. For example, for the interfacial type, one could rotate the configuration of Fig. 2 in space by $\pi/2$. This will leave the energy as well as the far field invariant.

IV. CHIRAL BIMERON PROFILE

For a quantitative study of the bimeron configuration, we consider a Möbius transformation defined by

$$\frac{1}{iw} = \frac{z - ia_1}{z - ia_2}, \tag{11}$$

where

$$w = u + iv$$

is the transformed variable in the complex plane. If this is applied to the configuration given in Eq. (8), we obtain

$$\Omega_S = \frac{1}{iw} = \frac{1}{r}\exp\left[-i\left(\frac{\phi + \pi}{2}\right)\right], \tag{12}$$

where (r, ϕ) are the polar coordinates for w. The result manifestly represents an axially symmetric antiskyrmion with a unit radius. Specifically, the Möbius transformation described by Eq. (11) shifts the antivortex center to the origin. An inversion is applied to the vortex configuration which is also reflected with respect to the real (horizontal) axis. This sets the vortex center to the point at infinity, and it reverses the sense of winding of the vortex configuration.

Chiral bimerons share with the configurations considered in Ref. [2] the salient property of being composed of merons with different radii (cf. Fig. 2), unlike the symmetric bimeron configurations of Eq. (8). To quantify this, we apply the Möbius transformation, i.e., Eq. (11), with a_1, a_2 chosen to coincide with the locations where $m_3 = \pm 1$, to our bimeron solutions $\Omega(z)$ and obtain

$$\tilde{\Omega}(w) = \Omega(z). \tag{13}$$

Figure 5 shows plots for $\tilde{\Omega}(w)$ corresponding to the transformation of the bimerons in Fig. 2. The resulting configurations are identified as skyrmions. The Möbius transformation maps the antivortex to the center of the skyrmion, whereas the vortex occupies the rest of the plane extending to spatial infinity. Approximately, the antivortex is mapped inside the circle $|w| = 1$ and the vortex outside it.

In Fig. 5, we observe circular vortex contours in the far field (corresponding to the vortex) and circular to elongated contours in the skyrmion center (corresponding to the antivortex). The dent in the shape of the contours below the skyrmion center is attributed to the region where $m_3 > 0$ below the antivortex, as noted in connection with Fig. 2 in Sec. III. Finally,

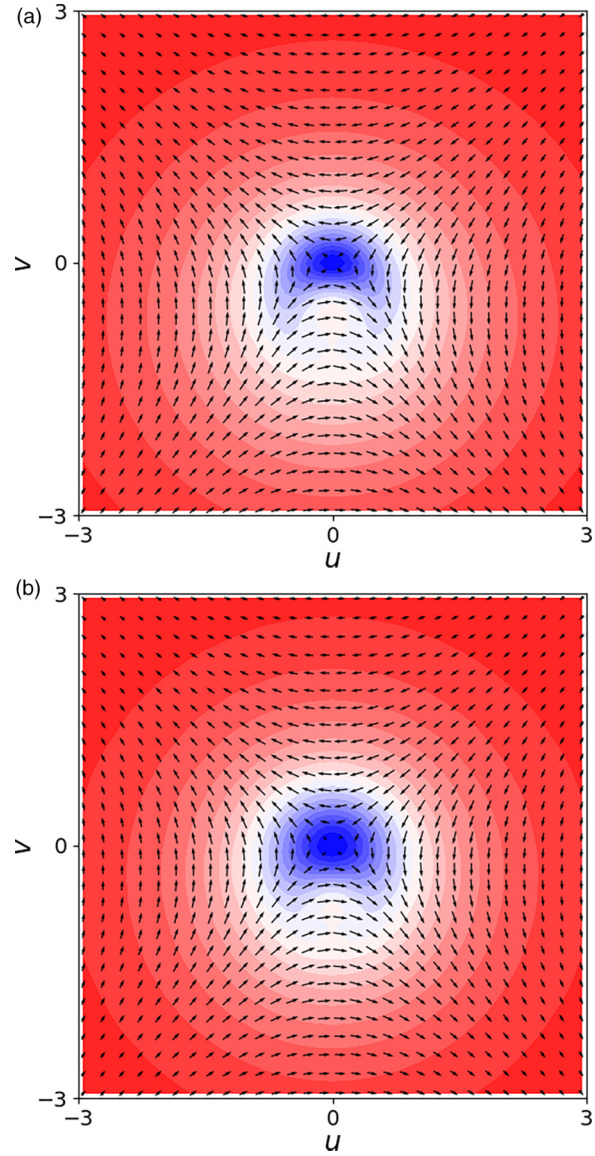

FIG. 5. (a) Vector and contour plots for the Möbius-transformed configuration given in Eq. (13) for the bimeron solutions of Fig. 2 for (a) $\lambda = 0.4$, and (b) $\lambda = 0.32$. The transformation has produced a skyrmion. Blue and red indicate $m_3 > 0$ and $m_3 < 0$, respectively. The antivortex has been mapped to the center of the skyrmion and the vortex to its periphery. The contours in the red region and in the central part of the blue region are approximately circles.

for smaller values of λ, the Möbius-transformed bimeron solutions $\tilde{\Omega}(w)$ approach progressively an axially symmetric profile as expected for the Belavin-Polyakov solution in Eq. (12).

We expect the radii of the two merons to be different and, in fact, the radius of the antivortex R_2 to be smaller than the radius R_1 of the vortex. Following the discussion in Ref. [2], we expect a Möbius-transformed configuration $\tilde{\Omega} = \gamma_2/(iw)$ around the center of the skyrmion and $\tilde{\Omega} = \gamma_1/(iw)$ in the outer region (for $|w| \gg 1$), with $\gamma_2 < \gamma_1$. This would imply vortex and antivortex radii $R_1 = R/\gamma_1$ and $R_2 = \gamma_2 R$, respectively, with R defined in Eq. (9). To detect this behavior in the chiral skyrmion configurations, we consider the relative

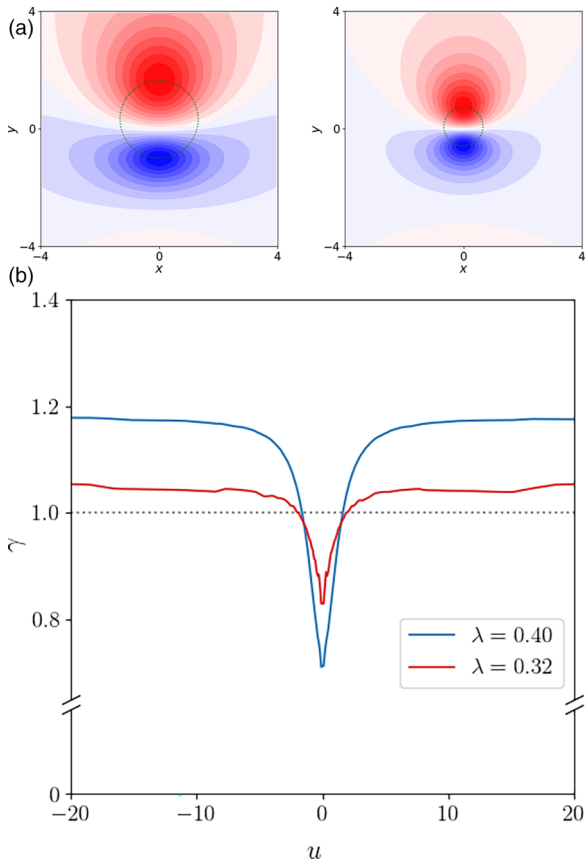

FIG. 6. (a) The dotted line shows the path for $v = 0$ on the z plane for $\lambda = 0.40$ (left) and $\lambda = 0.32$ (right). (b) The relative scaling γ [see Eq. (14)] is calculated along the u axis (for $v = 0$) for $\lambda = 0.40$ and 0.32. The value of γ obtained at $u = 0$ indicates the antivortex radius $R_2 = \gamma R < R$, and the value at $|u| \to \infty$ indicates the vortex radius $R_1 = R/\gamma < R$. They are both found to be smaller than the radius R given in Eq. (9) for the exchange model.

scaling:

$$\gamma := |w\tilde{\Omega}|, \tag{14}$$

which is expected to yield γ_1, γ_2 for the corresponding regions.

Figure 6(b) shows the scaling parameter γ as obtained along the horizontal u axis (i.e., the line $v = 0$) in Fig. 5 for the two values of λ. The saturation of the scaling parameter to $\gamma_1 > 1$ for $|u| \gg 1$ indicates a vortex radius $R_1 < R$. Similarly, for the antivortex, we find $\gamma_2 < 1$ for $u \ll 1$, corresponding to $R_2 < R$. For $\lambda = 0.32$, the values of γ_1, γ_2 are not very far from unity, showing that, in this case, the bimeron is close to the Belavin-Polyakov solution in Eq. (8). On the other hand, for $\lambda = 0.40$, the values of γ_1, γ_2 deviate significantly from unity, indicating that the individual meron sizes are shrinking compared with the total bimeron size, and they are thus progressively detaching from each other.

The separation of merons is in direct correspondence to the description in Ref. [2]. Related are also experimental reports in an easy-plane biaxial magnet where bubble domains are robustly observed [35]. Specifically, the so-termed *cyan bubble domain* contains two separated vortices or merons, and

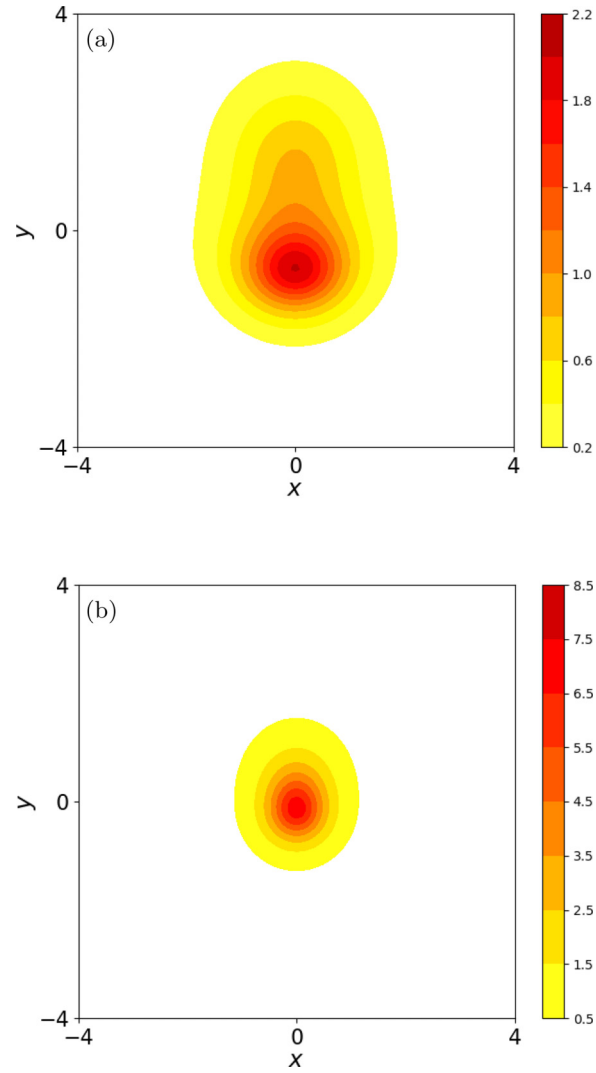

FIG. 7. Contour plots for the topological density q, defined in Eq. (6), of the bimeron solutions shown in Fig. 2 for (a) $\lambda = 0.4$ and (b) $\lambda = 0.32$. The same number of contours is plotted in both figures.

it can be considered the experimental realization of meron detachment.

Let us now proceed to consider the topological density distribution of the bimeron solutions. One should have in mind that the topological density for the rational map of Eq. (8) is axially symmetric (despite the asymmetry of the configuration). Figure 7 shows the topological density for the bimeron solutions of the two configurations in Fig. 2. For larger λ, the topological density distribution has an elongated shape with the two merons contributing in different parts of space. The topological density maximum is shifted to the antivortex side due to the sharper localization of the antivortex. As λ decreases, the topological density distribution approaches axial symmetry, and its center is shifted closer to the center of the bimeron (at the origin). These features further corroborate the assumption that the chiral bimeron approaches the configuration, see Eq. (12), for $\lambda \to 0$, while for large λ, the two merons detach from each other. A similar phenomenon was reported within a nonchiral model for anisotropic ferromagnets with competing interactions in Ref. [16].

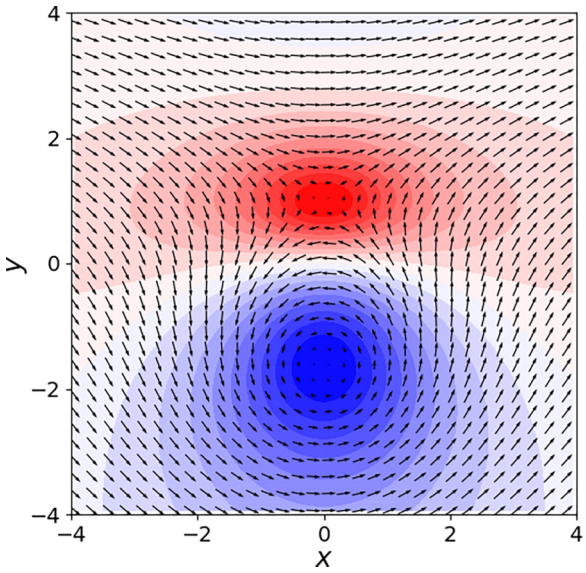

FIG. 8. A bimeron solution of the model given in Eq. (2) for $\lambda = 0.4$, where the vortex points down and the antivortex points up. Contour plots for m_3 are colored, where red indicates $m_3 > 0$ and blue indicates $m_3 < 0$. The center of the bimeron, defined to be at the point where $m_1 = -1$, has been placed at the origin. The skyrmion number is $Q = 1$.

V. BIMERON PAIRS

Considering the same system as in the previous sections, that is, retaining the vacuum magnetization $\mathbf{m} = \hat{\mathbf{e}}_1$, a second bimeron configuration can be found with an opposite skyrmion number. This has been noted in Refs. [7,11,36]. The second bimeron may be achieved by applying a rotation in space by π ($x \to -x, y \to -y$) and reversing the third magnetization component ($m_3 \to -m_3$) of the initial solution, in Fig. 2. The result, for $\lambda = 0.4$, is shown in Fig. 8. The vortex now has negative polarity, and the antivortex has positive polarity. This leads to a skyrmion number $Q = -1$, opposite the skyrmion number of the previously presented bimerons in Fig. 2. Thus, the easy-plane ferromagnet can support chiral bimerons with opposite skyrmion numbers.

A mechanism for the generation of bimerons can be readily suggested based on the existence of the two oppositely charged bimerons. One may imagine the generation of a vortex-antivortex pair where both vortices have the same polarity, say, down, with the simultaneous generation of a vortex-antivortex pair with polarity up [37]. Both pairs are topologically trivial, with $Q = 0$, and they can thus be created in a smooth way. An exchange of partners between the two pairs would give recombination of the vortices and antivortices such that two bimerons with opposite skyrmion numbers would emerge. When these unbind, they give the two bimerons in Figs. 2 and 8. A simulation demonstrating a pair of vortices together with a pair of antivortices, which may be interpreted as a pair of bimerons, was reported in Ref. [38].

We argue that the described mechanism may well be favored by the physics of the system because it has the following advantages. A topologically trivial vortex-antivortex pair can be created out of fluctuations of the polarized state. This pair is a propagating structure though [37], and it would eventually be annihilated via energy dissipation. On the other hand, a bimeron, once formed, is a static structure, that is, it is an energy minimum and thus a stable topological configuration that is robust against damping and perturbations.

Simulations showing bimeron generation by spin torques within an in-plane easy-axis model are reported in Ref. [36]. We give here a complementary proof-of-concept numerical simulation for bimeron generation. We consider an initially polarized state along the $\mathbf{m} = \hat{\mathbf{e}}_1$ direction, but we add a perturbation by setting $\mathbf{m} \approx (0.98, 0.2, 0)$ in the region $-2 \leqslant x, y \leqslant 1$. Spin-transfer torque of the Slonczewski type is then applied with polarization along x. This polarization is chosen because we aim for vortex-antivortex pairs where $\mathbf{m} \approx -\hat{\mathbf{e}}_1$ between the two vortices. The dynamics is described by

$$\partial_\tau \mathbf{m} = -\mathbf{m} \times \mathbf{h}_{\text{eff}} + \alpha \mathbf{m} \times \partial_\tau \mathbf{m} - \beta \mathbf{m} \times (\mathbf{m} \times \hat{\mathbf{e}}_1). \quad (15)$$

We set $\beta = -8$, and the polarized current is only applied in a circular region of radius 2 around the origin. The negative value of β corresponds to reversing the polarization to $-\hat{\mathbf{e}}_1$ or to reversing the direction of the current. We use the parameter value $\lambda = 0.4$ and damping $\alpha = 0.1$. A vortex-antivortex pair with negative polarity is created due to the dynamics, and it is shown in Fig. 9(a) at time $t = 20.0$.

Immediately after $t = 20.0$, we reverse the spin-torque parameter to $\beta = 8$. We see that a second vortex-antivortex pair, again with polarity down, is created, and soon after that, a third vortex-antivortex pair with polarity up starts growing. Figure 9(b) shows the configuration at $t = 20.6$. Then the antivortex from the third pair is annihilated with the vortex from the second pair, and the remaining vortex of the third pair binds with the antivortex of the first pair, as shown in Fig. 9(c), at time $t = 22.0$. The remaining vortex from the first pair and antivortex from the second pair have the same polarity; they approach each other, propagate away, and eventually annihilate smoothly. The picture in Fig. 9(d) shows the remaining bimeron at time $t = 28.0$.

The mechanism for the generation of two bimerons can be generalized to a process where a collection of bimerons is generated while the total skyrmion number of the system remains zero. If the temperature is considered, an easy-plane chiral magnet could give a gas of bimerons, leading to the question of a topological phase transition in the system. Given that the bimerons are static states, these will not only be sustained due to thermal fluctuations, but the system may be trapped in a state of multiple bimerons that may be a local energy minimum.

VI. CONCLUDING REMARKS

We have studied in detail chiral bimeron solutions in a magnet with a DM interaction. We found that they bear essential similarities to the bimerons originally discussed within the O(3) nonlinear sigma model, and we have quantified the similarity of the features employing a Möbius transformation of the bimeron configuration. The chiral bimerons thus appear to be a realization of the original bimeron configurations, presenting, for example, the possibility to detach from each other. This opens the possibility of the proliferation of merons under temperature or due to an external probe. We have described a

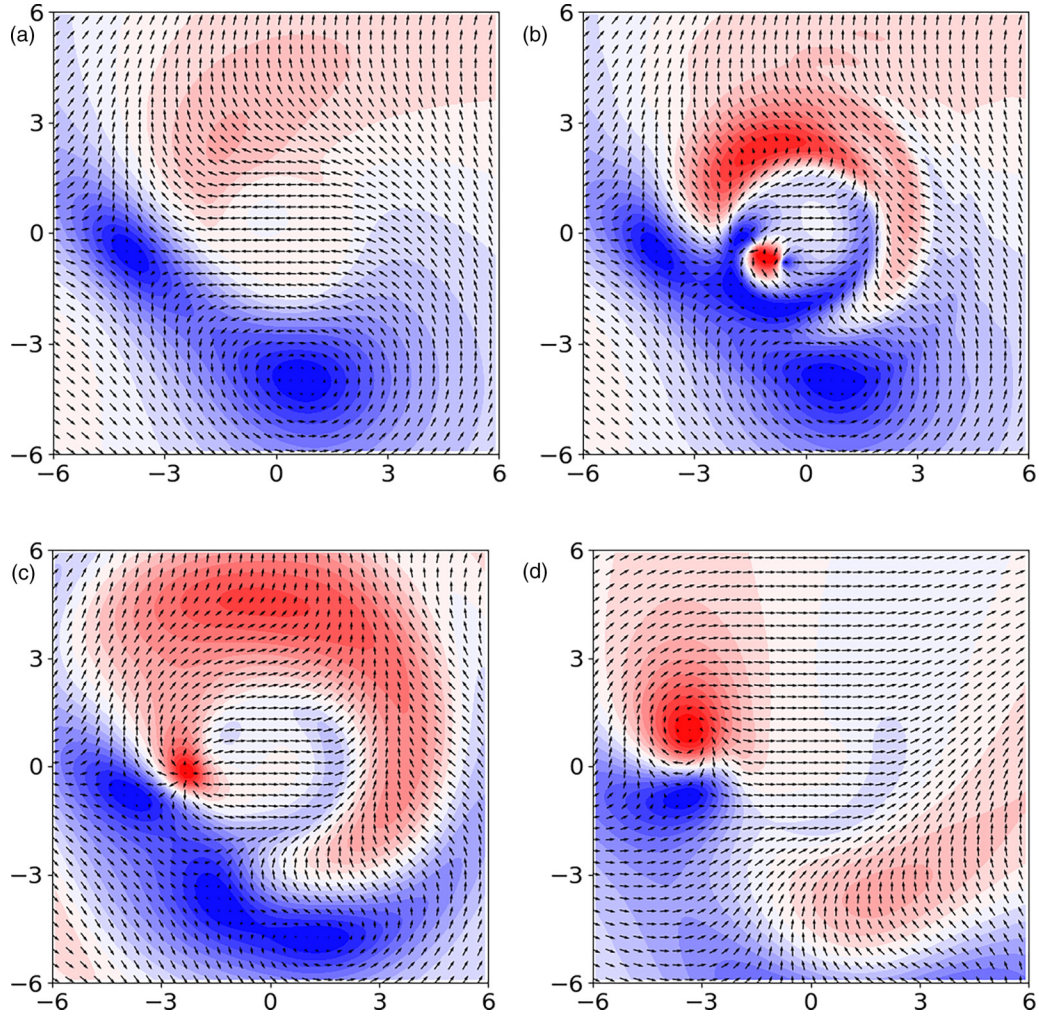

FIG. 9. Spin torque is applied on an almost polarized state. The following snapshots are shown. (a) A vortex-antivortex is generated, after the application of spin torque with $\beta = -8$ in a circular region with radius 2 for 20 time units. Following this stage, the polarization is reversed by setting $\beta = 8$, and we show snapshots at (b) $t = 20.6$, where a second vortex-antivortex pair with polarity down and a third one with polarity up are created, (c) $t = 22.0$, where a bimeron has been formed, and (d) $t = 28.0$, where only a single bimeron has remained in the system.

method and have given a proof-of-concept simulation for the generation of bimerons.

We have identified the range of parameters for the existence of bimerons and the configuration dependence on the parameter values. We further identified a special feature in the configuration, that is, the change of the sign of the out-of-plane magnetization component m_3 in the area beyond the antivortex.

A remarkable property of chiral bimerons is that they are static solutions of the model, unlike the situation in nonchiral magnets where vortex pairs are necessarily dynamical and they rotate around each other. The dynamics of chiral bimerons thus emerges as an interesting topic to study.

ACKNOWLEDGMENTS

We are grateful to Riccardo Tomasello for discussions on many of the issues discussed in this paper. This paper was supported by the project ThunderSKY funded by the Hellenic Foundation for Research and Innovation (HFRI) and the General Secretariat for Research and Innovation (GSRI), under Grant No. 871.

[1] C. G. Allan, Jr., R. Dashen, and D. J. Gross, A mechanism for quark confinement, Phys. Lett. B **66**, 375 (1977).

[2] D. J. Gross, Meron configurations in the two-dimensional O(3) σ-model, Nucl. Phys. B **132**, 439 (1978).

[3] A. N. Bogdanov and A. Hubert, Thermodynamically stable magnetic vortex states in magnetic crystals, J. Magn. Magn. Mater. **138**, 255 (1994).

[4] K. Everschor-Sitte, J. Masell, R. M. Reeve, and M. Kläui, Perspective: Magnetic skyrmions-overview of recent progress in an active research field, J. Appl. Phys. **124**, 240901 (2018).

[5] L. Bo, C. Hu, R. Zhao, and X. Zhang, Micromagnetic manipulation and spin excitation of skyrmionic structures, J. Phys. D **55**, 333001 (2022).

[6] A. O. Leonov and I. Kézsmárki, Asymmetric isolated skyrmions in polar magnets with easy-plane anisotropy, Phys. Rev. B **96**, 014423 (2017).

[7] K.-W. Moon, J. Yoon, C. Kim, and C. Hwang, Existence of in-Plane Magnetic Skyrmion and its Motion under Current Flow, Phys. Rev. Appl. **12**, 064054 (2019).

[8] N. Gao, S. G. Je, M. Y. Im, J. W. Choi, M. Yang, Q. Li, T. Y. Wang, S. Lee, H. S. Han, K. S. Lee *et al.*, Creation and annihilation of topological meron pairs in in-plane magnetized films, Nat. Commun. **10**, 5603 (2019).

[9] B. Göbel, A. Mook, J. Henk, I. Mertig, and O. A. Tretiakov, Magnetic bimerons as skyrmion analogues in in-plane magnets, Phys. Rev. B **99**, 060407(R) (2019).

[10] C. Xu, J. Feng, S. Prokhorenko, Y. Nahas, H. Xiang, and L. Bellaiche, Topological spin texture in Janus monolayers of the chromium trihalides Cr(I, X)$_3$, Phys. Rev. B **101**, 060404(R) (2020).

[11] R. Murooka, A. O. Leonov, K. Inoue, and J.-I. Ohe, Current-induced shuttlecock-like movement of non-axisymmetric chiral skyrmions, Sci. Rep. **10**, 396 (2020).

[12] B. Göbel, I. Mertig, and O. A. Tretiakov, Beyond skyrmions: Review and perspectives of alternative magnetic quasiparticles, Phys. Rep. **895**, 1 (2021).

[13] V. M. Kuchkin and N. S. Kiselev, Turning a chiral skyrmion inside out, Phys. Rev. B **101**, 064408 (2020).

[14] X. Li, L. Shen, Y. Bai, J. Wang, X. Zhang, J. Xia, M. Ezawa, O. A. Tretiakov, X. Xu, M. Mruczkiewicz *et al.*, Bimeron clusters in chiral antiferromagnets, npj Comput. Mater. **6**, 169 (2020).

[15] L. Shen, J. Xia, X. Zhang, M. Ezawa, O. A. Tretiakov, X. Liu, G. Zhao, and Y. Zhou, Current-Induced Dynamics and Chaos of Antiferromagnetic Bimerons, Phys. Rev. Lett. **124**, 037202 (2020).

[16] Y. A. Kharkov, O. P. Sushkov, and M. Mostovoy, Bound States of Skyrmions and Merons near the Lifshitz Point, Phys. Rev. Lett. **119**, 207201 (2017).

[17] S. K. Kim, Dynamics of bimeron skyrmions in easy-plane magnets induced by a spin supercurrent, Phys. Rev. B **99**, 224406 (2019).

[18] X. Zhang, J. Xia, L. Shen, M. Ezawa, O. A. Tretiakov, G. Zhao, X. Liu, and Y. Zhou, Static and dynamic properties of bimerons in a frustrated ferromagnetic monolayer, Phys. Rev. B **101**, 144435 (2020).

[19] H.-S. Han, S. Lee, M.-S. Jung, N. Kim, W. Chao, Y.-S. Yu, J.-I. Hong, K.-S. Lee, and M.-Y. Im, Topology-dependent stability of vortex-antivortex structures, Appl. Phys. Lett. **118**, 212407 (2021).

[20] H. Jani, J.-C. Lin, J. Chen, J. Harrison, F. Maccherozzi, J. Schad, S. Prakash, C.-B. Eom, A. Ariando, T. Venkatesan *et al.*, Antiferromagnetic half-skyrmions and bimerons at room temperature, Nature (London) **590**, 74 (2021).

[21] S. D. Yi, S. Onoda, N. Nagaosa, and J. H. Han, Skyrmions and anomalous Hall effect in a Dzyaloshinskii-Moriya spiral magnet, Phys. Rev. B **80**, 054416 (2009).

[22] X. Z. Yu, W. Koshibae, Y. Tokunaga, K. Shibata, Y. Taguchi, N. Nagaosa, and Y. Tokura, Transformation between meron and skyrmion topological spin textures in a chiral magnet, Nature (London) **564**, 95 (2018).

[23] X. Li and C. Melcher, Lattice solutions in a Ginzburg-Landau model for a chiral magnet, J. Nonlinear Sci. **30**, 3389 (2020).

[24] S. Mühlbauer, S. Gvasaliya, E. Ressouche, E. Pomjakushina, and A. Zheludev, Phase diagram of the Dzyaloshinskii-Moriya helimagnet $Ba_2CuGe_2O_7$ in canted magnetic fields, Phys. Rev. B **86**, 024417 (2012).

[25] J. Chovan, N. Papanicolaou, and S. Komineas, Intermediate phase in the spiral antiferromagnet $Ba_2CuGe_2O_7$, Phys. Rev. B **65**, 064433 (2002).

[26] S. Banerjee, J. Rowland, O. Erten, and M. Randeria, Enhanced Stability of Skyrmions in Two-Dimensional Chiral Magnets with Rashba Spin-Orbit Coupling, Phys. Rev. X **4**, 031045 (2014).

[27] J. Rowland, S. Banerjee, and M. Randeria, Skyrmions in chiral magnets with Rashba and Dresselhaus spin-orbit coupling, Phys. Rev. B **93**, 020404(R) (2016).

[28] S.-Z. Lin, A. Saxena, and C. D. Batista, Skyrmion fractionalization and merons in chiral magnets with easy-plane anisotropy, Phys. Rev. B **91**, 224407 (2015).

[29] M. Vousden, M. Albert, M. Beg, M.-A. Bisotti, R. Carey, D. Chernyshenko, D. Cortés-Ortuño, W. Wang, O. Hovorka, C. H. Marrows *et al.*, Skyrmions in thin films with easy-plane magnetocrystalline anisotropy, Appl. Phys. Lett. **108**, 132406 (2016).

[30] B. Schroers, Solvable models of magnetic skyrmions, in *Quantum Theory and Symmetries*, edited by M. B. Paranjape, R. MacKenzie, Z. Thomova, P. Winternitz, and W. Witczak-Krempa (Springer International Publishing, Cham, 2021), pp. 535–544.

[31] S. Komineas, C. Melcher, and S. Venakides, The profile of chiral skyrmions of small radius, Nonlinearity **33**, 3395 (2020).

[32] A. Bernand-Mantel, C. B. Muratov, and T. M. Simon, A quantitative description of skyrmions in ultrathin ferromagnetic films and rigidity of degree ± 1 harmonic maps from $\mathbb{R}^2 \to \mathbb{S}^2$, Arch. Ration. Mech. Anal. **239**, 219 (2021).

[33] V. L. Pokrovskii and G. V. Uimin, Dynamics of vortex pairs in a two-dimensional magnetic material, Pis'ma Zh. Eksp. Teor. Fiz. **41**, 105 (1985) [JETP Lett. **41**, 128 (1985)].

[34] S. Komineas, Rotating Vortex Dipoles in Ferromagnets, Phys. Rev. Lett. **99**, 117202 (2007).

[35] G. Chen, S. P. Kang, C. Ophus, A. T. N'Diaye, H. Y. Kwon, R. T. Qiu, C. Won, K. Liu, Y. Wu, and A. K. Schmid, Out-of-plane chiral domain wall spin-structures in ultrathin in-plane magnets, Nat. Commun. **8**, 15302 (2017).

[36] L. Shen, X. Li, J. Xia, L. Qiu, X. Zhang, O. A. Tretiakov, M. Ezawa, and Y. Zhou, Dynamics of ferromagnetic bimerons driven by spin currents and magnetic fields, Phys. Rev. B **102**, 104427 (2020).

[37] N. Papanicolaou and P. N. Spathis, Semitopological solitons in planar ferromagnets, Nonlinearity **12**, 285 (1999).

[38] S. A. Meynell, M. N. Wilson, K. L. Krycka, B. J. Kirby, H. Fritzsche, and T. L. Monchesky, Neutron study of in-plane skyrmions in MnSi thin films, Phys. Rev. B **96**, 054402 (2017).